Internal Concentration Gradients of Guest Molecules in Nanoporous Host Materials: Measurement and Microscopic Analysis

Pavel Kortunov,[†] Lars Heinke,*[,†] Sergey Vasenkov,[†,‡] Christian Chmelik,[†] Dhananjai B. Shah,[†,§] Jörg Kärger,[†] Rainer A. Rakoczy,[||] Yvonne Traa,[||] and Jens Weitkamp[||]

Fakultät für Physik und Geowissenschaften, Universität Leipzig, Linnéstr. 5, D-04103 Leipzig, Germany, Chemical Engineering Department, University of Florida, P.O. Box 116005, Gainesville, Florida 32611-6005, Chemical & Biomedical Engineering Department, Cleveland State University, 2121 Euclid Avenue, Cleveland, Ohio 44115-2214, and Institute of Chemical Technology, Universität Stuttgart, 70550 Stuttgart, Germany

Received: August 8, 2006; In Final Form: September 11, 2006

Evolution of internal concentration profiles of methanol in 2-D pore structure of ferrierite crystal was measured in the pressure range of 0 to 80 mbar with the help of the recently developed interference microscopy technique. The measured profiles showed that both a surface barrier and internal diffusion controlled the kinetics of adsorption/desorption. Furthermore, they indicated that in the main part of the crystal, the *z*-directional 10-ring channels were not accessible to methanol and that the transport of methanol mainly occurred via 8-ring *y*-directional channels. The roof-like part of the crystal was almost instantaneously filled/emptied during adsorption/desorption, indicating accessible 10-ring channels in this section. The measured profiles were analyzed microscopically with the direct application of Fick's second law, and the transport diffusivity of methanol in ferrierite was determined as a function of adsorbed phase concentration. The transport diffusivity varied by more than 2 orders of magnitude over the investigated pressure range. Transport diffusivities, calculated from measured profiles from small and large pressure step changes, were all found to be consistent. Simulated concentration profiles obtained from the solution of Fick's second law with the calculated functional dependence of diffusivities on concentration compared very well with the measured concentration profiles, indicating validity and consistency of the measured data and the calculated diffusivities. The results indicate the importance of measuring the evolution of concentration profiles as this information is vital in determining (1) the direction of internal transport, (2) the presence of internal structural defects, and (3) surface/internal transport barriers. Such detailed information is available neither from common macroscopic methods since, they measure changes in macroscopic properties and use model assumptions to predict the concentration profiles inside, nor from microscopic methods, since they only provide information on average displacement of diffusing molecules.

Introduction

Knowledge of transport in nanoporous materials is important for both fundamental understanding as well as practical aspects of design involving such materials. Zeolites, for example, are widely used as adsorbents and catalysts in chemical industry. Design of industrial adsorbers and/or catalytic reactors requires both the knowledge of diffusion transport mechanism and an accurate estimate of diffusivities in zeolites.[1−4]

Many different experimental techniques have been used to measure the rates of diffusion of different components in zeolites.[1,5,6] These methods can be broadly divided into two types: macroscopic[7] and microscopic.[8,9] In macroscopic methods, the changes in macroscopic quantities are measured upon imposed concentration change. For example, in gravimetric methods, the weight of the sample is measured as a function of time. In chromatographic methods, the concentration of adsorbate in the fluid stream exiting the column is monitored as a function of time. The measured changes in external macroscopic properties are usually several mass transfer steps removed from the internal diffusion. For example, in gravimetric methods, other transport resistances such as external film, macropore diffusion and external heat transfer may be present. In chromatographic measurements, axial dispersion, external film resistance, and macropore diffusional resistances are present. To determine internal transport diffusivities from these measurements, several assumptions have to be made about the intervening mass transfer resistances and experiments have to be performed under conditions where these assumptions are valid. Micropore diffusivities from these methods are deduced but are never measured directly from internal concentration profiles. Model assumptions regarding the mechanism of transport play a major role in the information deduced on the internal transport. The literature is full of examples where experimental conditions did not match the assumptions made in the model development for data analysis resulting in erroneous values of transport diffusivities.[10] In a more recent publication,[11] we have shown how erroneous interpretation of such measurements can be and how they can lead to a wrong physical picture of transport inside the porous structure. Presence of structural defects and/or surface/internal transport barriers can drastically change the

* Corresponding author. E-mail address: heinke@physik.uni-leipzig.de.
[†] Universität Leipzig.
[‡] University of Florida.
[§] Cleveland State University.
[||] Universität Stuttgart.

10.1021/jp065112c CCC: $33.50
Published on Web 10/18/2006

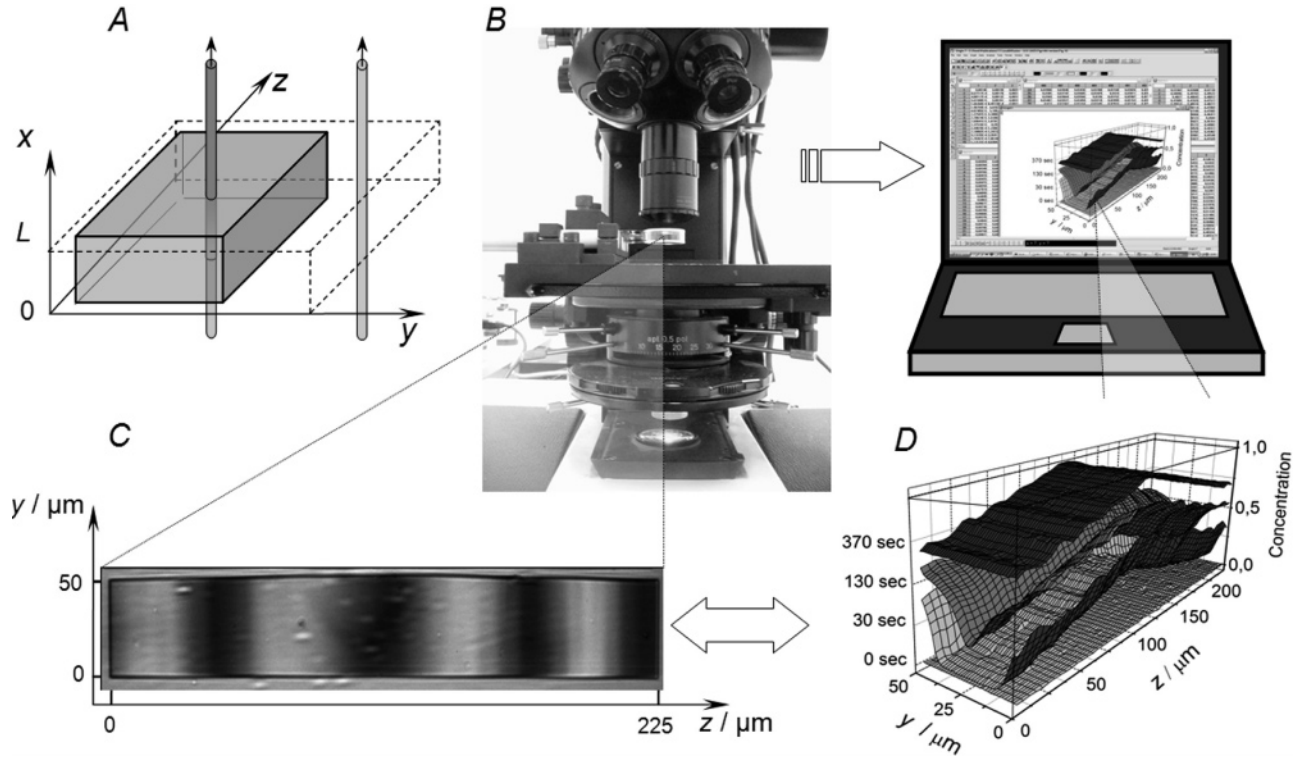

Figure 1. Schematics of the interference microscopy method. (A) Light beams passing through the crystal and through the surrounding atmosphere. (B) The interference microscope. (C) Interference patterns generated due to different optical properties. (D) Evolution of the concentration profiles calculated from the changes in interference patterns with time.

internal transport that the macroscopic methods are not able to measure or predict unequivocally.[12,13]

Microscopic methods such as quasi elastic neutron scattering (QENS) and pulsed field gradient nuclear magnetic resonance (PFG NMR), on the other hand, monitor internal displacement of molecules and hence provide more direct measurement of internal transport. Examples abound in the literature where discrepancies of several orders of magnitude exist between the diffusivities measured by the two sets of methods for the same adsorbate−adsorbent systems.[1,5,14,15] However, these microscopic methods only provide measurements of average molecular displacement over the sample.[16] They do not provide information on the distribution of guest molecules in the porous materials. Even the NMR imaging techniques,[17] used extensively for medical diagnoses, are not capable of providing internal measurements of how concentration profiles evolve with time with the required spatial and temporal resolution.

Ideally, therefore, an experimental technique is needed that is capable of measuring internal concentration profiles as a function of distance and time. The recently developed interference microscopy technique has the ability to monitor the internal concentration profiles with the required spatial and temporal resolution.[18] With this experimental technique, it is possible to calculate diffusivities from the measured internal profiles without making any model assumptions about other mass transfer processes. In addition, the measured profiles can give direct evidence of internal transport mechanism and can help identify internal structural defects and/or presence of surface/internal barriers.

In this contribution, we report on the extensive set of measurements we have made by interference microscopy of methanol concentration profiles in a ferrierite crystal with a spatial resolution of about 1 μm and temporal resolution of 10 s. The internal concentration profiles have been measured for different pressure steps and for both adsorption and desorption. The Fick's second law has been directly applied to these measured profiles and the internal transport diffusivities have been calculated as a function of adsorbed phase concentration. The results have been checked by comparing the experimental concentration profiles with those simulated from the solution of Fick's second law with the calculated diffusivity values and their dependence on adsorbed phase concentration as input values.

Experimental Section

The measurements were performed by the interference microscopy method which uses the principle that optical density of light passing through a transparent crystal is dependent on the nature and amount of guest molecules present in the crystal. Two light beams are used: one passing through the sample and the other passing through the surrounding atmosphere (Figure 1A). The analysis of interference patterns (and hence the phase shift) emerging from the superposition of these two beams provides the concentration profile (Figures 1B through 1D). The concentrations so calculated are average concentrations in the direction of the light beam. The spatial resolution perpendicular to the light beam is limited by the diffraction of the light (about 0.5 μm). However, such a resolution is more than sufficient if relatively large crystals are used in the experiments. More details on the theoretical aspects of interference microscopy can be found elsewhere.[18]

The experimental setup consists of an optical vacuum cell containing zeolite crystals. The cell is connected to a vacuum system with a stock volume of about 2 L to execute pressure step changes during adsorption and desorption. The step changes are accomplished within a fraction of a second, and the final pressure is maintained constant at the desired values. A Carl-Zeiss JENAPOL interference microscope with interferometer of Mach−Zender type has been used for the measurements. The

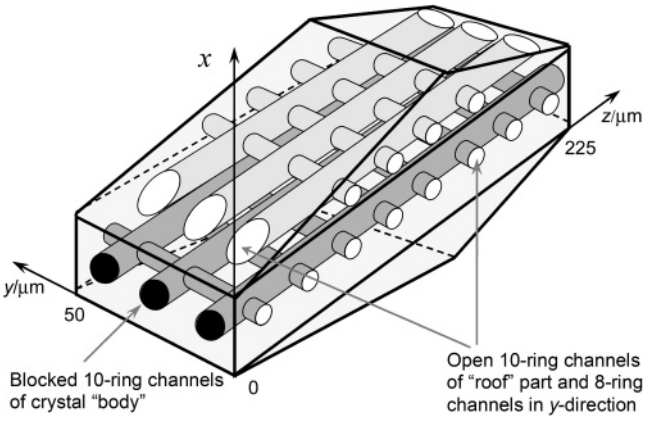

Figure 2. Ferrierite crystal with a two-dimensional pore structure. The figure shows partially blocked *z*-direction channels in the main body of the crystal, open *z*-direction channels in the roof section, and open *y*-direction channels.

interference patterns are recorded by a CCD camera (Sony XC-77CE) monitoring interference between the crystal and the surrounding. Compared to the time constants of a few thousand seconds for the observed adsorption/desorption processes, the present experimental setup provides time resolution of 10 seconds allowing for a very detailed monitoring of the evolution of the concentration profiles.

The zeolite crystals studied were the cation-free silica ferrierite of about 50 μm × 200 μm × 10 μm size and a shape of a rectangular solid body with a "roof" on both elongated sides (Figure 2). They were synthesized at the University of Stuttgart. They were activated under high vacuum at a temperature of 400 °C for 12 h. To ensure that there are no organic residues, the activation was preceded by exposing the sample to oxygen at 700 °C for 4 h.

All experiments were performed at room temperature with one selected crystal. The adsorbate used was pure methanol (obtained from Sigma-Aldrich, 99.9% purity with largest impurity being water at < 0.03%). The experiments were performed between the pressure steps from 0 → 5, 5 →10, 0 → 10, 0 →20, 0 → 40, and 0 → 80 mbar and, correspondingly, desorption steps used were initiated by the same pressure steps in backward direction.

Results

Qualitative Observations. The ferrierite crystals exhibit a two-dimensional channel structure with a wider, "ten-membered" ring (formed by 10 silica and 10 oxygen atoms) channels along the *z*-direction with an elliptical cross section of 0.54 nm × 0.42 nm. There are smaller, "eight-membered" ring channels along the *y*-direction with an elliptical cross section of 0.48 nm × 0.35 nm. The smaller *y*-direction channels intersect the bigger channels, and there are 12 such intersections per unit cell. Unless structural defects exist in the crystal lattice, there should be no transport in the *x*-direction as there exist no channels in this direction. Based on the structure of the ferrierite crystal, one expects to find concentration gradients in *y* and *z* directions but none in the *x*-direction (direction of the light beams).

The measured concentration profiles are shown in Figure 3 for the pressure step of 0 to 80 mbar at times of 30, 130, and 370 s. Figure 3A shows the evolution of 2-D concentration profiles in *y* and *z* directions. Figures 3B and 3C show the evolution of the concentration profiles in *z* and *y* directions, respectively.

The profiles in the *z*-direction pretty much mirror the geometry of the roof section. The maximum concentration in the center is due to the shape of the crystal as the optical path in the center of the crystal is larger than that at the edges. The *z*-concentration profiles were, therefore, corrected by subtracting the final equilibrium intensity at each point. The corrected profiles, after an initial transient, were nearly flat over the length of the crystal. Since well-defined concentration profiles exist in *y*-direction, it appears that the roof-like section of the crystal is filled up almost instantaneously (within 30 s) through the wider, ten-membered ring channels during adsorption. It is similarly emptied equally fast during desorption. However, the main part of the crystal is filled mainly by diffusion in *y*-direction. Hence, one has to conclude that the 10-ring channels in the main part of the crystal body are blocked or are inaccessible but they are open in the roof-like section of the crystal. This is illustrated in Figure 2. It shows the crystal morphology as well as the open and blocked channels as deduced from the observed concentration profiles. Thus, methanol diffusion in ferrierite crystals exhibits roughly a one-dimensional behavior in the main part of the crystal.

It is noteworthy that the concentration at $y = 0$ and 50 μm do not immediately attain the equilibrium concentration. One has to conclude, therefore, that in addition to the very pronounced transport barriers at $z = 0$ and $z = 225$ μm, essentially precluding diffusion in *z*-direction, there are also transport resistances at the entrances of the eight-membered channels in the *y*-direction.

It is important to recognize that interference microscopy provides concentration values in relative units of intensity and not in terms of absolute amounts. The intensity at equilibrium for each pressure step is known from the measurements. To convert the measured intensities into absolute amounts adsorbed, we performed similar adsorption/desorption experiments using infrared (IR) microspectroscopy. The results from IR measurements were used to estimate the absolute amount adsorbed at 80 mbar (4 mmol/gm). This conversion was used along with IFM measurements of intensity to estimate the adsorption isotherm. It is shown in Figure 4.

Microscopic Analysis

1. Transport Diffusivities from 1-D Analysis. For analyzing the evolution of concentration profiles of guest molecules, we start with Fick's second law for one-dimensional diffusion in *y*-direction. It takes the form

$$\frac{\partial c(y,t)}{\partial t} = \frac{\partial}{\partial y}\left(D(c(y,t))\frac{\partial c(y,t)}{\partial y}\right) = \frac{\partial D(c(y,t))}{\partial c}\left(\frac{\partial c(y,t)}{\partial y}\right)^2 + D(c(y,t))\frac{\partial^2 c(y,t)}{\partial y^2} \quad (1)$$

In this equation, D is the transport diffusivity. The concentration c in the crystal depends only on time t and space coordinate y. Since concentration is measured at different y and t by interference microscopy, it is, in principle, possible to calculate the transport diffusivity and its concentration dependence by careful analysis.

The first term on the right-hand side vanishes in the middle of the crystal since the first spatial derivative is necessarily zero there due to crystal symmetry. Hence,

$$D_{\text{center}} \approx \frac{\partial c/\partial t}{\partial^2 c/\partial y^2} \quad (2)$$

It is, therefore, possible to get an initial estimate of diffusivity and its concentration dependence by analysis of profiles at the

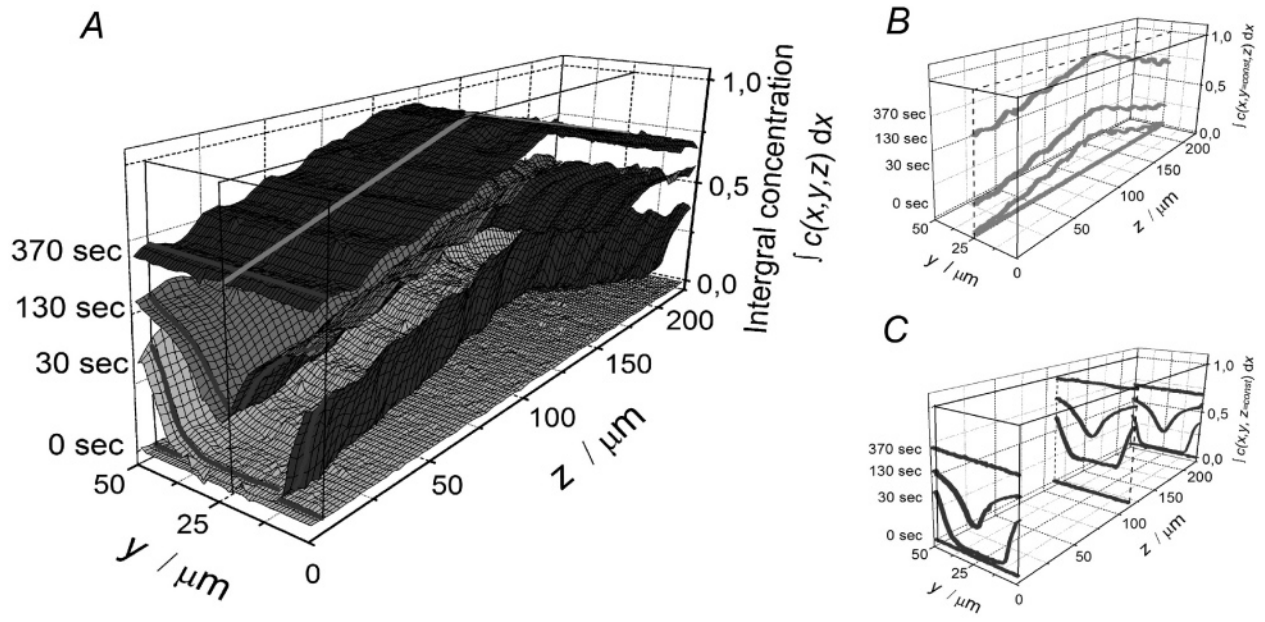

Figure 3. Concentration profiles measured during adsorption for the pressure step of 0 → 80 mbar. The concentration is normalized with respect to the maximum value in the roof. (A−C) Concentration profiles. (B) Concentration profiles in the *z*-direction.(C) Concentration profile in the *y*-direction.

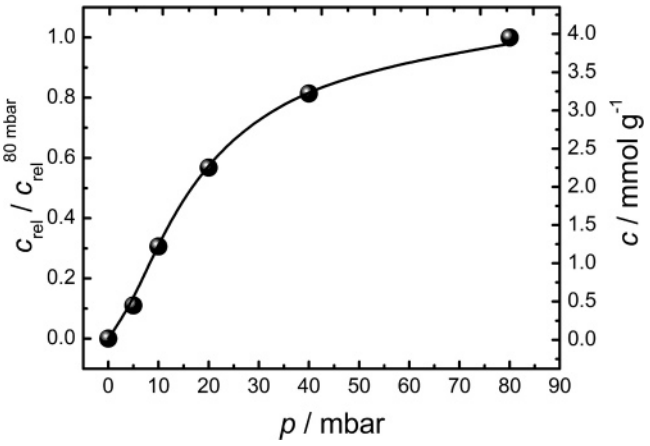

Figure 4. Adsorption isotherm of methanol on ferrierite as determined from interference microscopy with the absolute amount adsorbed calculated based on infrared microscopy.

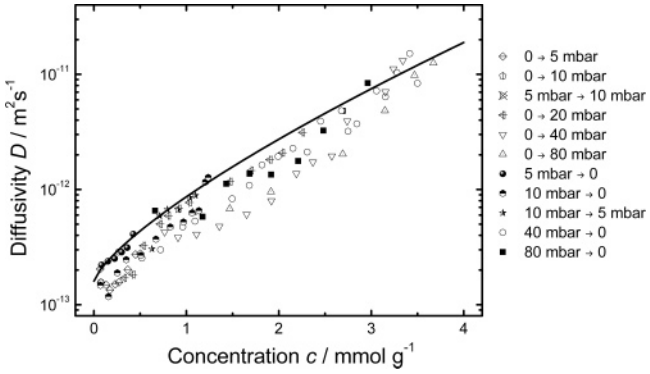

Figure 5. Transport diffusivity in the *y*-direction as a function of concentration obtained from the center of the crystal from different experiments. The full line represents the concentration dependence used for calculations leading to the concentration profiles in Figures 7 and 8.

center of the crystal. The derivatives can be calculated from the concentration profiles numerically or analytically. The concentration profiles were measured initially at about every 30 s and then the time increments were increased as equilibrium was approached. The knowledge of concentration profiles at two different times is sufficient to approximate numerically the derivatives in eq 2. Our approach was to fit the concentration profiles, at each time, to an analytical expression and then differentiate the derived expression to determine the first and second spatial derivatives at any position *y*. Similarly, concentrations at a particular *y*, but, at different times, were also fitted to an analytical expression and the expression was differentiated to obtain $\partial c/\partial t$. The concentration profiles in the middle when analyzed in this manner provide the values of transport diffusivities at different concentrations. The results are shown in Figure 5. The eq 1 can now be applied to all other points in the crystal and the initially determined concentration dependency can be used to estimate $\partial D/\partial c$ to obtain a better estimate of transport diffusivity and its concentration dependence. The results obtained from the analysis of concentration profiles over the entire concentration range and for all positions are shown in Figure 6 for the pressure step of 0 to 40 mbar.

Figures 5 and 6 show a strong dependence of transport diffusivity on concentration. The diffusivities vary by more than 2 orders of magnitude over the concentration range. It is important to note that the concentration range covered is quite high (corresponding to pressure steps of 0 to 80 mbar). The diffusivities do show scatter and, at a given concentration, differ by as much as a factor of 2. The scatter is to be expected because of the extensive data set generated for each experiment. For every pressure step, on an average, concentration profiles at 10 different times have been generated. A horizontal line at a given concentration intersects a number of concentration profiles, and each profile will provide a value for transport diffusivity at that concentration. However, the most remarkable aspect of Figure 5 is that it contains diffusivities calculated from all experiments (those with small and large pressure changes). Moreover, when Figures 5 and 6 are superimposed on one another, the two diffusivity bands overlap. This indicates that the intracrystalline transport diffusivity *D* of the adsorbed phase for all performed pressure steps is a unique function of the concentration. The transport diffusivities calculated from the center are consistent

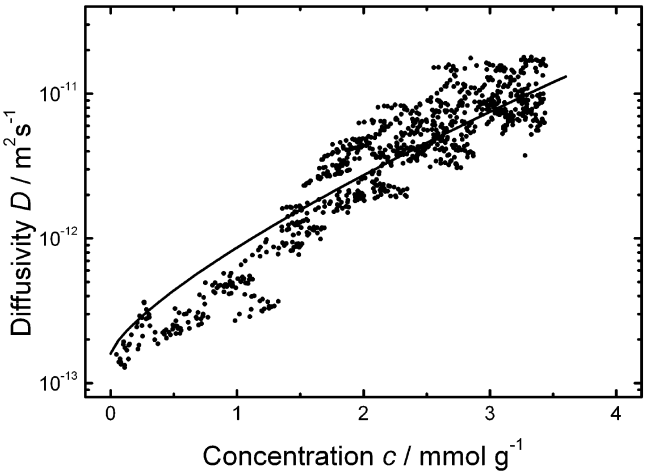

Figure 6. Transport diffusivity determined from all profiles over the entire crystal region for the desorption step from 40 mbar to vacuum with the same concentration dependency as derived from results in Figure 5. The full line represents the concentration dependence used for calculations leading to the concentration profiles in Figures 7 and 8.

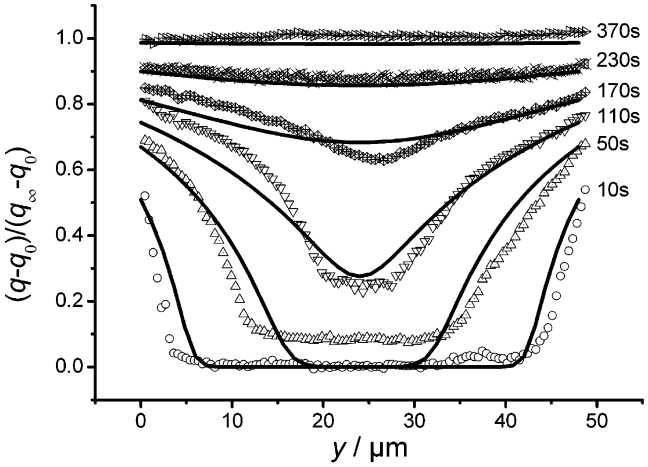

Figure 7. Comparison of simulated and experimental profiles for the adsorption step from 0 to 80 mbar. The dots are experimental measurements. The lines are simulated from 1-D finite difference solution with the same concentration dependence of transport diffusivities as determined from Figures 5 and 6 (full lines).

with those calculated from other positions. One may, therefore, use the approximate analysis at the center with reasonable confidence to determine transport diffusivities and their dependence on concentration.

2. Surface Barrier/Resistance. The profiles show that surface barriers exist in both *y* and *z* directions because the relative concentrations at the edge do not instantaneously attain the equilibrium values 1 and 0, corresponding to adsorption and desorption, respectively. It is possible to determine the permeability α of the surface by relating the flux *J* through an edge with the concentration difference between the equilibrium value at the surface and the one measured at the edge (eq 3).

$$J_y \propto \frac{1}{2}\frac{\partial m}{\partial t} = \frac{1}{2}\frac{\partial\left(\int_{-l}^{l}\frac{c}{2l}\mathrm{d}y\right)}{\partial t} = \alpha_y(c_e - c) \qquad (3)$$

Here c_e is the concentration in equilibrium with the pressure in the optical cell, J_y is the flux through a face of the crystal at $y = 0$ or $y = 50$ μm, c is the measured concentration at the edge, m is the mass of adsorbate in the crystal at time t averaged over y, $2l$ is the crystal extension in y-direction and α_y is the surface permeability. The factor 1/2 arises because the adsorbate amount in the crystal increases due to diffusion through two opposing faces. Using eq 3, α_y was calculated for each profile. Similar calculations were also performed for α_z, the surface permeability in the *z*-direction.

The determination of surface permeabilities α on the basis of eq 3 implies that the actual difference between the measured concentration, *c*, close to the crystal boundary and the equilibrium concentration, c_e, is not affected by heat effects during the process of adsorption. An estimate of this influence is presented elsewhere[19] and confirms the justification of this assumption.

The calculated surface permeabilities are of the order of 10^{-8} to 10^{-7} m/s. They are found to be a function of the pressure step, i.e., of both the equilibrium concentration and the actual concentration close to the crystal surface. The calculated surface permeability of the big ten-membered ring channels is much smaller than that in the *y*-direction, indicating that the entrances to the channels in the *z*-direction are essentially blocked. The whole uptake is dominated by diffusion along the smaller eight-membered ring channels with bigger surface permeability. This explains why, in the main part of the crystal, methanol diffusion in ferrierite may be considered as to proceed in a one-dimensional system.

The calculated values of α_y and α_z showed no particular pattern. They varied with concentration and were not equal for adsorption and desorption. A concentration dependent surface permeability is difficult to interpret with the simple picture of blocked or partially obstructed channels. The surface barrier may be due to a combination of factors such as presence of surface defects, partially blocked channels, presence of a thin layer with lower diffusivity below the surface, etc. However, the true nature of surface resistance cannot be gauged from our measurements. Hence, no attempt is made to provide any physical interpretation to these quantities based on their magnitudes and their functional dependence on concentration. Instead, the surface permeabilities α_y and α_z have been used and considered as mere fitting parameters to fix the surface concentrations correctly at each time. In the subsequent section, we show the excellent agreement between the measured concentration profiles and their evolution predicted on the basis of Fick's second law with the deduced diffusivities and permeabilities.

3. Comparison of Simulated and Experimental Profiles − 1-D versus 2-D Diffusion. To check the accuracy of the microscopically calculated intracrystalline transport diffusivity and its concentration dependence, we simulated the evolution of concentration profiles by numerically solving the 1-D Fick's second law with the surface permeabilities and transport diffusivities calculated earlier as input. These simulated profiles for the case of 0 to 80 mbar adsorption step are compared with the measured profiles in Figure 7. It is clear that the simulated profiles for 10, 50, 110, and 170 s do a poor job of representing the measured concentration profiles.

The measured profiles show higher concentrations at the edge as well as higher concentrations in the central region. The adsorption profiles in the beginning of the adsorption run show a region of horizontal flat concentration profile (for example at time 10, 50, and 110 s). The length of the horizontal flat region decreases with time. This is expected as a consequence of methanol diffusion further and further into the crystallite interior. However, the concentrations in this flat central region increase with time (about 0.0 at 10 s, 0.08 at 50 s and 0.25 at 110 s). If

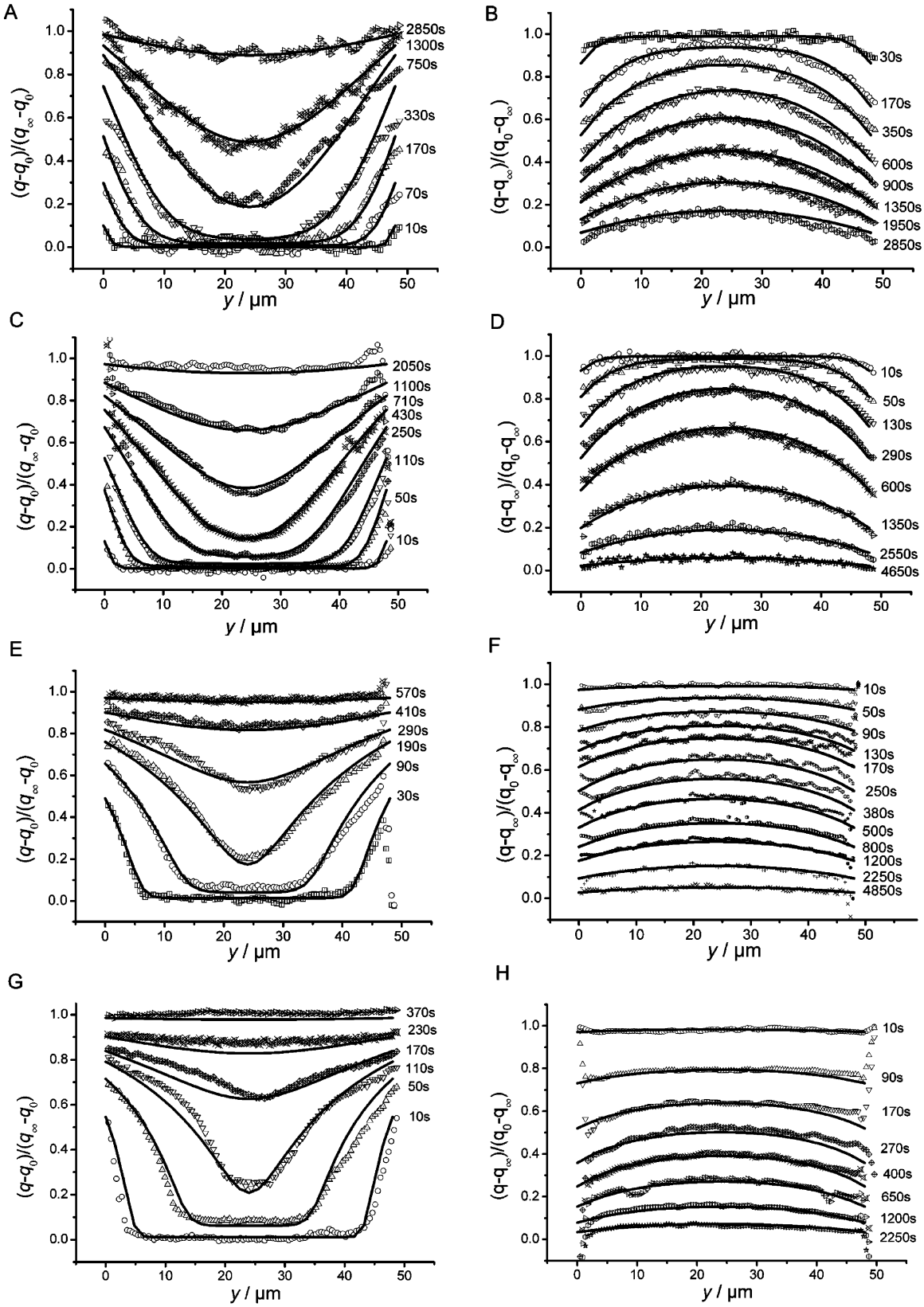

Figure 8. Comparison of simulated and experimental profiles for pressure steps 0 to 5 mbar (A), 5 to 0 mbar (B), 0 to 10 mbar (C), 10 to 0 mbar (D), 0 to 40 mbar (E), 40 to 0 mbar (F), 0 to 80 mbar (G), and 80 to 0 mbar (H). The points are experimental measurements. The lines are simulated from 2-D finite difference solution with the same concentration dependence of transport diffusivities as determined from Figures 5 and 6 (full lines) and the surface permeabilities determined from the use of eq 3. The value of D_z used in simulation is $\gg D_y$.

transport in the *y*-direction were solely responsible for increasing methanol concentration in the crystal, one would not expect increasing concentrations corresponding to the flat profiles. There should be very little increase of concentration in the middle region since there are no *y*-gradients in this region. This increasing concentration without any *y*-gradient can occur only if fluxes from other directions are present. Since there is no flux in the *x*-direction due to the absence of channels in that

direction, it implies that the flux from the *z*-direction needs to be accounted for to correctly simulate the concentration profiles.

We may assume that transport of methanol in the *z*-direction is governed solely by surface barrier. This is indicated by a substantial drop in concentration at the crystal edge from the equilibrium value (indicated by a relatively small value of α_z). The internal *z*-profiles are relatively flat indicating fast diffusion through bigger ten-member rings (a relatively large value of D_z compared to D_y). Hence there is no measurable concentration gradient along the *z*-direction.

With this rationale, Fick's second law was numerically solved for two-dimensional diffusion with $D_y = f(c)$, $\alpha_y = f(c)$, and $\alpha_z = f(c)$ determined earlier and $D_z = 5 \times 10^{-11}$ m^2/s, a value 2 orders of magnitude higher than that for D_y. The results are shown in Figures 8A−H. With this method, all measured data can be excellently simulated with one concentration-dependent diffusivity function along the *y*-direction and one high-diffusivity value along the *z*-direction for all pressure steps.

The shape of the measured profiles changes with the magnitude of the pressure step change, nicely reflecting the relevance of range of the local diffusivities covered during the experiment. When the imposed pressure step is small (Figures 8A−D) the adsorption profiles appear parabolic assuming the shape well-known from textbook patterns for constant diffusivity.[20] However, for higher pressure step changes (Figures 8E−H), the concentration profiles exhibit initially a flat central region which gradually dissipates and the profiles show a v-shape (Figure 3B, profile at 130 s). On the other hand, desorption profiles get significantly flatter with increasing pressure step changes. Similarly, desorption for small pressure step changes proceeds almost as fast as adsorption as resulting from basic diffusion theory. At higher step changes, however, desorption is almost 10 times slower. Such a behavior may be easily rationalized considering the dramatic concentration dependence of the diffusivity as reflected by Figures 5 and 6. As the adsorbed phase concentration increases, transport diffusivity increases significantly and is about 2 orders of magnitude higher than that at low concentrations. This explains why adsorption is much more rapid than the corresponding desorption for high pressure steps and the resulting concentration profiles are not symmetrical. For small pressure step changes, the adsorption and desorption processes are nearly symmetrical because the transport diffusivity is nearly constant in the considered interval.

Furthermore, the changing shapes of adsorption concentration profiles from near parabolic shapes for small pressure changes (Figures 8A and 8C) to ones with deep-valley shape (Figures 8E and 8G) can be easily explained by the effect of strongly increasing diffusivity with concentration. Due to the initial low concentration in the crystal, the resulting diffusivity is small. Higher concentrations near the crystal surface result in a much higher diffusivity and hence a much faster increase there. These differences are magnified with increasing pressure.

During the desorption process, the diffusivity is high in the beginning due to high concentration. This high diffusivity relatively quickly evens the concentration profiles in the bulk of the crystal and the resulting profiles are much flatter. Near the crystal surface, the concentration is low due to zero relative concentration at the surface. This results in low diffusivity near the surface resulting in slow release of the adsorbate. This explains why desorption process is so slow compared to adsorption.

Conclusions

The concentration profiles of methanol in a ferrierite crystal measured by interference microscopy indicate that the diffusion is almost one-dimensional. These profiles were analyzed microscopically by Fick's second law. First, the measured concentration profiles were analyzed at the center to yield the complete concentration dependence of the transport diffusivities in a first iteration. These values were then verified and confirmed by analyzing the concentration profiles over the whole crystal. The results obtained were consistent since the same transport diffusivity values, and their concentration dependence was calculated for all measured adsorption and desorption steps. The calculated transport diffusivity ranged from 10^{-13} to 10^{-11} m^2 s^{-1} and was found to increase substantially with increasing concentration.

The measured profiles were compared with the simulated profiles by solving Fick's second law with the determined diffusivity-concentration function. The agreement over all the pressure steps was excellent.

The measured evolution of concentration profiles allowed us to infer the transport processes taking place in the ferrierite crystal. It showed that the 10-membered channels are nearly blocked in the main part of the crystal but open in the roof-like structure. This results in a filling/emptying of the roof section almost instantaneously on adsorption/desorption. It also showed that the majority of uptake in the crystal is accomplished by filling through the smaller eight-membered channels. The overall diffusion process in ferrierite can be satisfactorily described as one-dimensional diffusion.

Such detailed information on the transport process is necessary to determine the dominant direction and rate of mass transfer and to explore the presence of structural defects and surface barriers. Interference microscopic measurements enable us to measure the evolution of internal concentration profiles with time and allow us to determine local microscopic diffusivities. Macroscopic methods and microscopic methods such as QENS and PFG NMR are not able to provide such measurements. Development of this method has the potential to make significant fundamental contributions to understanding of transport mechanisms in nanoporous materials.

The method described here is applicable to relatively large crystals that are transparent to light. Moreover, it also requires that adsorption is slow enough to track the evolution of concentration profiles. One can judiciously choose the adsorbent−adsorbate systems where the process of diffusion is sufficiently slow to effectively measure the progress of the diffusion process. This can be accomplished relatively easily for a variety of systems, as has been demonstrated in previously published papers from our laboratory.[21−25]

Acknowledgment. The authors acknowledge Prof. D. M. Ruthven for stimulating discussions. Financial support by Deutsche Forschungsgemeinschaft (Gast-Mercator award to D.B.S., IRTG "Diffusion in porous media", IRG "Diffusion in Zeolites"), Fonds der Chemischen Industrie and Max-Buchner-Forschungs-Stiftung is gratefully acknowledged.

References and Notes

(1) Ruthven, D. M. *Principles of adsorption and adsorption processes*; Wiley & Sons: New York, 1984.

(2) Yang, R. T. *Gas separation by adsorption processes*; Butterworth: Boston, 1987.

(3) Chen, N. Y.; Degnan, T. F.; Smith, C. M. *Molecular transport and reaction in zeolites*; VCH: New York, 1994.

(4) Ruthven, D. M.; Farooq, S.; Knaebel, K. S. *Pressure swing adsorption*: VCH: New York, 1994.

(5) Karger, J.; Ruthven, D. M. *Diffusion in zeolites and other microporous solids*; John Wiley: New York, 1992.

(6) Karger, J.; Ruthven, D. M. in *Handbook of porous materials*; Schüth, F., Sing, K. S. W., Weitkamp, J., Eds.; Wiley-VCH: Weinheim, Germany, 2002; Vol. 4, 2089−2173.

(7) Ruthven, D. M.; Brandani, S. in *Physical adsorption: experiment, theory and applications*; Fraissard, J. Ed.; Kluwer Academic Publishers: Netherlands, 1997; pp 261−296.

(8) Karger, J.; Freude, D. *Chem. Eng. Technol*. **2002**, *25*, 769−778.

(9) Kärger, J.; Vasenkov, S. in *Host−Guest systems based on nanoporous crystals*; Laeri, F., Schüth, F., Simon, U., Wark, M., Eds.; Wiley-VCH: Weinheim, Germany, 2003; pp 255−279.

(10) Kärger, J.; Ruthven, D. M. *Zeolites* **1989**, *9*, 267−281.

(11) Kortunov, P.; Chmelik, C.; Kärger, J.; Rakoczy, R. A.; Ruthven, D. M.; Traa, Y.; Vasenkov, S.; Weitkamp, J. *Adsorption* **2005**, *11*, 235−244.

(12) Chmelik, C.; Kortunov, P.; Vasenkov, S.; Kärger, J. *Adsorption* **2005**, *11*, 455−460.

(13) Kortunov, P.; Vasenkov, S.; Chmelik, C.; Kärger, J.; Ruthven, D. M.; Wloch, J. *Chem. Mater.* **2004**, *16*, 3552−3558.

(14) Kärger, J. *Adsorption* **2003**, *9*, 29−35.

(15) Kärger, J. *Ind. Eng. Chem. Res.* **2002**, *41*, 3335−3340.

(16) Kärger, J.; Valiullin, R.; Vasenkov, S. *New J. Phys.* **2005**, *7*, 1−15.

(17) Callaghan, P. T. *Principles of NMR microscopy*; Clarendon Press: Oxford, 1991.

(18) Schemmert, U.; Kärger, J.; Weitkamp, J. *Microporous Mesoporous Mater*. **1999**, *32*, 101−110.

(19) Heinke, L.; Chmelik, C.; Kortunov, P.; Shah, D. B.; Brandani, S.; Ruthven, D. M.; Kärger, J., *Microporous Mesoporous Mater*. **2006**, accepted.

(20) Crank, J. *Mathematics of Diffusion*, 2nd ed.; Oxford University Press: Oxford, 1975.

(21) Kortunov, P.; Vasenkov, S.; Chmelik, C.; Kärger, J.; Ruthven, D. M.; Wloch, J. *Chem. Mater*. **2004**, *16*, 3552−3558.

(22) Kortunov, P.; Chmelik, C.; Kärger, J.; Rakoczy, R. A.; Ruthven, D. M.; Traa, Y.; Vasenkov, S.; Weitkamp, J. *Adsorption* **2005**, *11*, 235−244.

(23) Lehmann, E.; Chmelik, C.; Scheidt, H.; Vasenkov, S.; Staudte, B.; Kärger, J.; Kremer, F.; Zadrozna, G.; Kornatowski, J. *J. Am. Chem. Soc.* **2002**, *124*, 8690−8695.

(24) Lehmann, E.; Vasenkov, S.; Kärger, J.; Zadrozna, G.; Kornatowski, J.; Weiss, Ö.; Schüth, F. *J. Phys. Chem. B* **2003**, *107*, 4685−4687.

(25) Lehmann, E.; Vasenkov, S.; Kärger, J.; Zadrozna, G.; Kornatowski, J. *J. Chem. Phys. B* **2003**, *118*, 6129−6132.